

Critical Parameter Design for a Cascaded H-Bridge With Selective Harmonic Elimination/Compensation Based on Harmonic Envelope Analysis for Single-Phase Systems

Hui Zhao , *Student Member, IEEE*, Shuo Wang , *Senior Member, IEEE*, and Amirhossein Moeini , *Student Member, IEEE*

Abstract—This paper investigates the critical parameter design technique for a cascaded H-Bridge (CHB) with selective harmonic elimination (SHE)/compensation (SHC) for single-phase systems. The critical parameters include the filter inductance, the number of H-bridge cells, the dc-bus voltage and the switching frequency. This paper derives the relationship of electrical parameters, topologies, and modulation techniques to the voltage/current harmonic envelopes, and compares the filter inductor design for an H-Bridge with sinusoidal pulsewidth modulation (SPWM), an H-Bridge (HB) with SHE/SHC and a CHB with SHE/SHC. Furthermore, a harmonic-envelope-based approach is developed to determine the optimum design parameters. The developed approach designs the harmonic envelope with two proposed criteria: the first one is the capacity criterion, which guarantees that the fundamental and controllable components are within the applicable solution range to avoid overmodulation; the other one is the attenuation criterion, which ensures that the uncontrollable harmonic complies with the grid limit. Simulations and experiments verified that a CHB designed with the proposed technique can simultaneously fulfill the compensation objectives and meet the harmonic limits.

Index Terms—Cascaded H-Bridge (CHB), compensation capacity, critical parameter design, filter design, harmonic analysis, harmonic attenuation requirement, selective harmonic elimination (SHE), compensation (SHC).

I. INTRODUCTION

A CASCADED H-Bridge (CHB) with selective harmonic elimination (SHE)/compensation (SHC) is a promising candidate in modular high-power electronics applications, such as grid-tied photovoltaic (PV) inverters, wind farms, and electric vehicle charging stations [1]–[3]. A CHB with SHE can control fundamental component to absorb/inject active power [4]–[8], to

Manuscript received January 10, 2018; revised April 6, 2018; accepted May 15, 2018. Date of publication June 7, 2018; date of current version November 30, 2018. This work was supported by the National Science Foundation under Grant 1540118. (*Corresponding author: Shuo Wang.*)

The authors are with the Department of Electrical and Computer Engineering, University of Florida, Gainesville, FL 32611 USA (e-mail: zhaohui@ufl.edu; shuowang@ieee.org; ahm1367@ufl.edu).

Color versions of one or more of the figures in this paper are available online at <http://ieeexplore.ieee.org>.

Digital Object Identifier 10.1109/TIE.2018.2842759

TABLE I
CRITICAL PARAMETERS IN A CHB CIRCUIT

Number of cells	DC voltage of each cell	Filter inductance	Number of switching transitions
N	E	L	K

compensate reactive power [5], [9] and to compensate the three-phase unbalanced currents [10]. Furthermore, a CHB with SHC can also inject the selected high-order harmonics to compensate grid high-order harmonics [5], [11]–[13] as active power filters (APFs).

Although all the objectives in [4]–[13] can be fulfilled, the design of critical parameters, such as filter parameters, number of cells, switching frequencies, and dc-bus voltages is obscure. Existing techniques mainly focus on the parameter [14]–[17], circuit structure [15] and the modeling [18] of the coupling filters (for simplification, filters will be used to represent coupling filters in the later part of the paper) between CHBs and the power grid. Rockhill *et al.* [16] and Zabaleta *et al.* [17] investigate the filter design based on switching frequencies in low-switching frequency applications. However, the critical parameter design also depends on circuit topologies and modulation techniques. A new design procedure should be developed.

CHB circuits have more critical parameters to design than an H-Bridge (HB) circuit, as given in Table I, so it is necessary to investigate how each parameter influences the current/voltage harmonics.

The output voltage of H-Bridge has harmonics. In this paper controllable harmonics are defined as the harmonics whose magnitude and phase can be controlled with the switching angles of the staircase waveforms in SHE/SHC or with the modulation reference signal in sinusoidal pulsewidth modulation (SPWM). The fundamental is also controllable. Not all harmonics are controllable due to the limited number of switching angles in SHE/SHC or the limited switching frequency in SPWM. The harmonics out of control are defined as uncontrollable harmonics in this paper.

With SPWM, the closed-form expression for harmonics and the required filter insertion loss can be derived [16], [19]. The most critical harmonics which determine the filter design are

close to the equivalent switching frequencies of the CHB and the expression for their magnitudes has been derived. So, the filter can be designed based on critical harmonics. However, SHE/SHC is a numerical algorithm and only focuses on the selected harmonics. All other harmonics are uncontrollable. The uncontrollable harmonics are widespread in the spectrum, and their magnitudes are unknown. As a result, the filter cannot be easily designed.

Most literature such as [17] design filters based on trial-and-error to meet the grid limit. But, this procedure is very time-consuming and lacks the theoretical understanding of the filter, as a result, the size/volume of the inverters is not optimized.

In the SHE/SHC of [8], [10]–[13], the uncontrollable current harmonics cannot comply with the grid limit. For the SHE in [4] and [7], only selective voltage harmonics are eliminated, and it is uncertain if the currents resulted from the uncontrollable voltage harmonics can meet the grid limit. For the SHE in [6], the filters are overdesigned as all current harmonics are far below the grid limit. Current mitigation techniques [9] can comply with the grid limit, but the exhaustion method is used.

Another critical issue is that filter design mainly considers how to attenuate the uncontrollable harmonics [14]–[18]. However, critical parameter design depends on not only the uncontrollable harmonics, but also controllable the fundamental and harmonics. In this paper, the envelope of the fundamental and controllable harmonics is defined as compensation capacity of the CHB; and the filter's attenuation to uncontrollable harmonics is defined as attenuation ability. It is well known that a large filter not only increases attenuation ability, but also decreases the compensation capacity. Therefore, the design of the compensation capacity and the design of the attenuation ability are a dilemma. Other parameters such as switching frequency and the number of cells must be considered in filter design, otherwise it is difficult to meet both the compensation capacity and attenuation ability requirement.

This paper explores the relationship of critical parameters, topologies, and modulation techniques to the envelopes of voltage/current harmonics. Based on the harmonic envelope, the paper developed a simple and straightforward technique to design all critical circuit parameters for CHBs with SHE/SHC. With the designed parameters, CHBs with SHE/SHC can meet both compensation capacity and attenuation ability requirements.

The paper is organized as follows. Section II analyzes and compares the harmonics of three different techniques: one HB with SPWM, one HB with SHE/SHC, and a CHB with SHE/SHC. Section III proposes two criteria for parameter design: The criterion for compensation capacity and the criterion for attenuation ability. A design technique is developed for critical parameters to guarantee that the output currents can meet both criteria. In Section IV, simulations and experiments are conducted to verify that the parameters designed with the proposed technique can fulfill the compensation capacity, and the uncontrollable harmonics can meet the harmonic limits.

II. HARMONIC ANALYSIS AND COMPARISON

This section will analyze the voltage/current spectrum for different topologies with different modulations. The harmonic

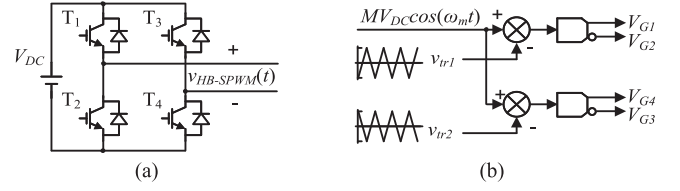


Fig. 1. Topology and modulation principle of an HB with SPWM. (a) Circuit topology. (b) Modulation diagram.

envelope is critical in parameter design. Appropriate parameters shall guarantee that the compensation capacity is large enough (i.e., the envelope of the fundamental and controllable harmonics should be greater than the reference of the voltage/current of a CHB), and the attenuation ability is enough (i.e., the maximum uncontrollable harmonic is below the harmonic limits). Because the compensation capacity is determined by the fundamental component and controllable harmonics, while the harmonic attenuation requirement is determined by the magnitude difference of the uncontrollable harmonics and the harmonic limits, this section separates the whole frequency range into two sections: the controllable harmonic frequency range which includes the fundamental frequency component and controllable harmonics, and the uncontrollable harmonic frequency range. Therefore, the controllable frequency range, the envelope of the magnitude of the controllable harmonics and the envelope of the magnitude of the uncontrollable harmonics will be investigated.

A. HB With SPWM technique

The topology and modulation principle of an HB with SPWM are shown in Fig. 1. The harmonics of the output voltage can be derived with dual Fourier analysis [19]. The modulation with naturally sampled reference and double-edge carrier is given as an example here. The output voltage of CHB is mostly determined by the modulation component and the sideband harmonics of the carrier (switching) frequency as given by

$$\begin{aligned}
 v_{HB-SPWM}(t) &\approx \underbrace{MV_{DC} \cos(\omega_m t)}_{\text{Modulation Component}} \\
 &+ \underbrace{\frac{2}{\pi} V_{DC} \sum_{n=-\infty}^{\infty} J_{2n-1}(\pi M) \cos(n\pi) \cos((2\omega_C + (2n-1)\omega_m)t)}_{\text{SideBand Harmonics}} \\
 &= v_{M_HB-SPWM}(t) + v_{H_HB-SPWM}(t) \quad (1)
 \end{aligned}$$

where n is the baseband index [16], which is related to the sideband harmonics, M is the modulation index, V_{DC} is the dc-bus voltage of the HB, ω_m is the modulation frequency which could be equal to grid frequency ω_g or a grid harmonic to be controllable, $\omega_C = K\omega_g$ is the carrier (switching) frequency, and $J_{2n-1}(\pi M)$ is the Bessel function [19]. The sidebands of switching harmonics are ignored in (1) as their magnitudes are much smaller than that of fundamental switching frequency.

In (1), $v_{M_HB-SPWM}(t) = MV_{DC} \cos(\omega_m t)$ is the controllable modulation component, and the magnitude $|V_{M_HB-SPWM}|$ is MV_{DC} . M should be smaller than one. Also, $v_{H_HB-SPWM}(t) = \frac{2}{\pi} V_{DC} \sum_{n=-\infty}^{\infty} J_{2n-1}(\pi M) \cos(n\pi) \cos((2\omega_C + (2n-1)\omega_m)t)$

is the uncontrollable sideband harmonics. Their frequencies equal to $2\omega_C + (2n - 1)\omega_m$. The magnitude represented by $|V_{H_HB-SPWM}|$ equals to $2V_{DC}|J_{2n-1}(\pi M)|/\pi$. Because $|J_{2n-1}(\pi M)| \leq 0.5819$ and it reaches the maximum value when $M = 0.5860$ and $n = 0$ or 1 , the frequencies of the highest harmonics are $\omega = (2\omega_C - \omega_m)$ and $(2\omega_C + \omega_m)$ [19]. The maximum magnitude is $|V_{H_HB-SPWM}|_{\max} = 0.5819V_{DC} \times 2/\pi = 0.3704V_{DC}$.

Generally, when the controllable frequency range includes not only ω_g , but also the harmonics of ω_g , the envelope of the maximum voltage spectrum of all modulation conditions is given by

$$\begin{cases} |V_{M_HB-SPWM}|_{\max} = V_{DC} & \omega \leq \omega_{HB-SPWM-CPS} \quad (2) \\ |V_{H_HB-SPWM}|_{\max} = 0.3704V_{DC} & \omega = (2\omega_C \mp \omega_m) \quad (3) \end{cases}$$

where $\omega_{HB-SPWM-CPS}$ is the maximum controllable frequency range. If single inductor L_{FLT} is used as the filter, the current envelope can be expressed as (4), (5) and (6) as shown at the bottom of this page, where, $I_{F_HB-SPWM}$ is the fundamental current component, $I_{M_HB-SPWM}$ is the controllable current harmonic, $I_{H_HB-SPWM}$ is the uncontrollable current harmonic, and $h = \omega_m/\omega_g$ is the harmonic order of grid frequency.

Because $|J_{2n-1}(\pi M)/(2\omega_C + (2n - 1)\omega_m)|$ reaches the maximum when $M = 0.5860$ and $n = 0$, the maximum current harmonic can be derived from (6)

$$|I_{H_HB-SPWM}|_{\max} = 0.3704V_{DC}/(2\omega_C - \omega_m)L_{FLT}. \quad (7)$$

Choose the base value as $V_{base} = V_{DC}$, $Z_{base} = \omega_g L_{FLT}$, then the per-unit voltage and current envelopes are given by (8)–(12), respectively, as shown at the bottom of this page.

The controllable frequency range, $\omega_{HB-SPWM-CPS}$, is limited by several factors, including the limitation derived from the sampling theorem, the phase delay caused by modulation process and the energy band of the uncontrollable harmonics [22]. A common range employed in industrial applications is

$$\omega_{HB-SPWM-CPS} = \omega_C/5 = K\omega_g/5. \quad (13)$$

$$\begin{cases} |I_{F_HB-SPWM}|_{\max} = \frac{(V_{DC} - V_g)}{\omega_g L_{FLT}} & \omega_m = \omega_g \quad (4) \\ |I_{M_HB-SPWM}|_{\max} = \frac{V_{DC}}{\omega_m L_{FLT}} = \frac{V_{DC}}{h\omega_g L_{FLT}} & 3\omega_g \leq \omega_m \leq \omega_{HB-SPWM-CPS} \quad (5) \\ |I_{H_HB-SPWM}|_{\max} = \frac{2V_{DC}}{\pi L_{FLT}} \left| \frac{J_{2n-1}(\pi M)}{2\omega_C + (2n - 1)\omega_m} \right| & \omega \geq \omega_{HB-SPWM-CPS} \quad (6) \end{cases}$$

$$\begin{cases} |V_{M_HB-SPWM}|_{\max}^p = 1 & \omega_m \leq \omega_{HB-SPWM-CPS} \quad (8) \\ |V_{H_HB-SPWM}|_{\max}^p = 0.3704 & \omega = (2\omega_C \mp \omega_m) \quad (9) \end{cases}$$

$$\begin{cases} |I_{F_HB-SPWM}|_{\max}^p = (V_{DC} - V_g)/V_{DC} & \omega_m = \omega_g \quad (10) \\ |I_{M_HB-SPWM}|_{\max}^p = 1/h & 3\omega_g \leq \omega_m \leq \omega_{HB-SPWM-CPS} \quad (11) \\ |I_{H_HB-SPWM}|_{\max}^p = 0.3704/h & \omega = 2\omega_C - \omega_m. \quad (12) \end{cases}$$

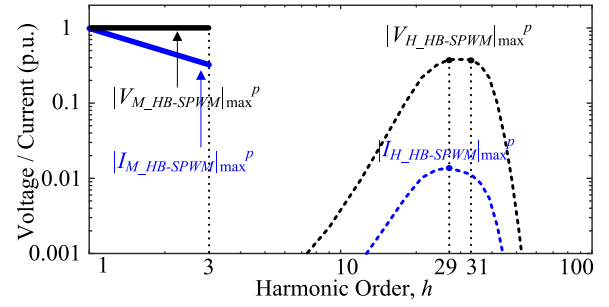


Fig. 2. Per unit voltage and current spectrum envelopes of an HB with SPWM ($K = 15$, $\omega_m = \omega_g$).

As an example, the voltage and current envelopes are shown in Fig. 2 with $\omega_C = 15\omega_g$. The solid lines represent the controllable envelopes for voltage (black) and current (blue), and they are calculated from (8) and (11). The dot lines represent the uncontrollable switching harmonics which should be attenuated. As shown in (1), the maximum voltage magnitude is $2V_{DC}|J_{2n-1}(\pi M)|/\pi$ for the harmonic at frequency $2\omega_C + (2n - 1)\omega_C$. The maximum value of Bessel function $|J_{2+1}(\pi M)|$ with $M \leq 1$ can be calculated using MATLAB. The envelope of the sideband harmonics looks asymmetrical because x -axis is in log-scale.

It is assumed in (1) that modulation component has only one frequency. For APFs which control multiple grid harmonics, [20] derived the closed-form expression for sideband harmonics, and proved that the highest magnitude of the uncontrollable harmonics is smaller than (1). The sideband harmonics in (1) are thus the worst scenario for filter design.

B. HB With SHE/SHC

The half-wave symmetry modulation is used as an example. The topology and waveform are shown in Fig. 3. The switching

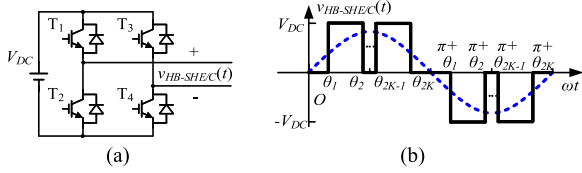


Fig. 3. Topology and waveform of an HB with SHE/SHC modulation. (a) Circuit topology. (b) Output voltage waveform.

frequency is $K\omega_g$. The maximum harmonic is derived (A9)

$$|V_{\text{HB-SHE}/C}|_{\text{max}} = \begin{cases} 4V_{\text{DC}}/\pi, & h \leq K \\ 4KV_{\text{DC}}/h\pi, & h \geq K \end{cases}. \quad (14)$$

The envelope of the maximum output current with inductor L_{FLT} as a filter is, therefore

$$|I_{\text{HB-SHE}/C}|_{\text{max}} = \begin{cases} [(4V_{\text{DC}}/\pi) - V_g]/(\omega_g L_{\text{FLT}}), & h = 1 \\ 4V_{\text{DC}}/(h\pi\omega_g L_{\text{FLT}}), & 3 \leq h < K \\ 4KV_{\text{DC}}/(h^2\pi\omega_g L_{\text{FLT}}), & h \geq K \end{cases}. \quad (15)$$

Similar to Section II-A, the base values are selected as $V_{\text{base}} = V_{\text{DC}}$, $Z_{\text{base}} = \omega_g L_{\text{FLT}}$. The per-unit voltage/current envelopes are

$$|V_{\text{HB-SHE}/C}|_{\text{max}}^p = \begin{cases} 4/\pi, & h < K \\ 4K/(h\pi), & h \geq K \end{cases} \quad (16)$$

$$|I_{\text{HB-SHE}/C}|_{\text{max}}^p = \begin{cases} 4/\pi - V_g/V_{\text{DC}}, & h = 1 \\ 4/(h\pi), & 1 \leq h < K \\ 4K/(h^2\pi), & h \geq K \end{cases}. \quad (17)$$

For the controllable frequency range, the total number of the controllable harmonics of SHE/SHC equals to K . Because a filter has large attenuation in high-frequency range, to fully utilize its attenuation ability, most applications choose low-frequency harmonics as the controllable harmonics. The frequencies of the controllable harmonics are $\omega_g, 3\omega_g, \dots, (2K-1)\omega_g$. Even order harmonics are zero because of half waveform symmetry. The range of the controllable harmonics is, therefore, $[0, \omega_{\text{HB-SHE}/C-\text{CPS}}]$, where,

$$\omega_{\text{HB-SHE}/C-\text{CPS}} = 2K\omega_g. \quad (18)$$

The voltage and current spectrum envelopes are shown in Fig. 4 when $K = 15$ from (16) and (17).

C. CHB With SHE/SHC

The topology and waveform of a CHB with SHE/SHC is shown in Fig. 5. Similar to Section II-B, the half-wave symmetrical modulation is used as an example. The maximum harmonic

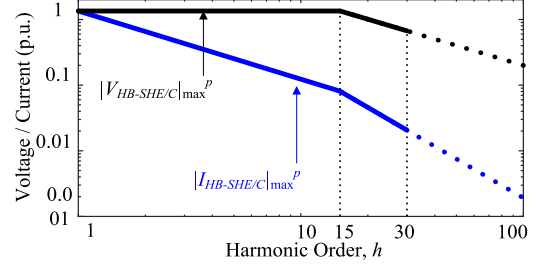


Fig. 4. Per unit voltage and current spectrum envelopes of an HB with SHE/SHC ($K = 15$).

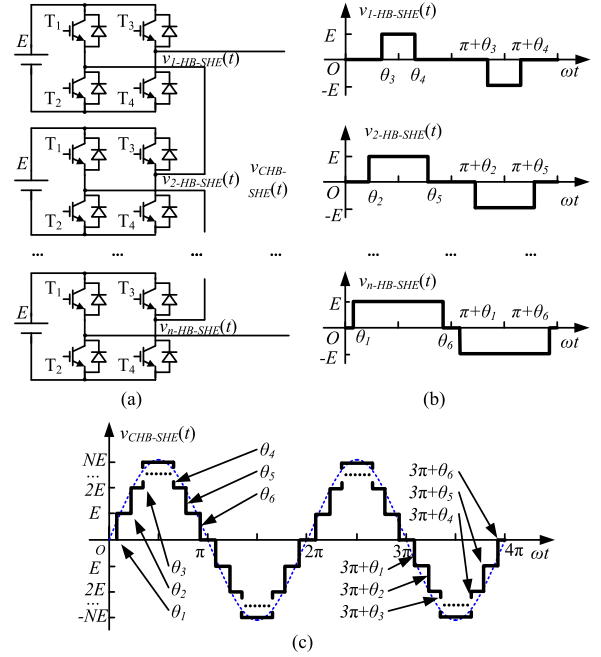


Fig. 5. Topology and waveform of a CHB with SHE/SHC. (a) Circuit topology. (b) Output voltage of each cell. (c) Overall output voltage $v_{\text{CHB-SHE}/C}$.

is derived in the Appendix as (A14)

$$|V_{\text{CHB-SHE}/C}|_{\text{max}} = \min\left(\frac{4KE}{h\pi}, \frac{4NE}{\pi}\right) = \begin{cases} 4NE/\pi, & h < K/N \\ 4KE/(h\pi), & h \geq K/N \end{cases} \quad (19)$$

$$|I_{\text{CHB-SHE}/C}|_{\text{max}} = \begin{cases} [(4NE/\pi) - V_g]/(\omega_g L_{\text{FLT}}), & h = 1 \\ 4NE/(h\pi\omega_g L_{\text{FLT}}), & 3 \leq h < K/N \\ 4KE/(h^2\pi\omega_g L_{\text{FLT}}), & h \geq K/N \end{cases}. \quad (20)$$

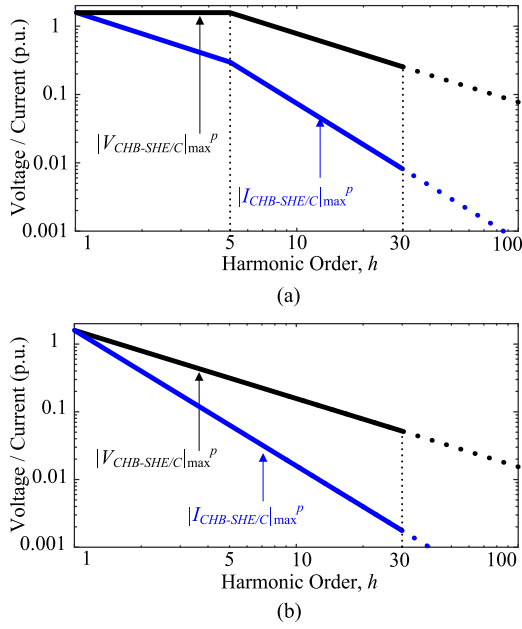


Fig. 6. Per unit voltage and current spectrum envelopes of a CHB with SHE/SHC. (a) $N = 3, K = 15$. (b) $N = 15, K = 15$ (staircase).

Choosing $V_{\text{base}} = NE$, $Z_{\text{base}} = \omega_g L_{\text{FLT}}$ as base values, the per-unit voltage and current envelopes are

$$|V_{\text{CHB-SHE/C}}|_{\max}^p = \begin{cases} 4/\pi, & h < K/N \\ 4K/(h\pi N), & h \geq K/N \end{cases} \quad (21)$$

$$|I_{\text{CHB-SHE/C}}|_{\max}^p = \begin{cases} 4/\pi - V_g/(NE), & h = 1 \\ 4/(h\pi), & 3 \leq h < K/N \\ 4K/(h^2\pi N), & h \geq K/N \end{cases} \quad (22)$$

The controllable harmonic range is $[0, \omega_{\text{CHB-SHE/C-CPS}}]$, and is determined by the number of switching transitions K

$$\omega_{\text{CHB-SHE/C-CPS}} = 2K\omega_g. \quad (23)$$

Fig. 6 shows the envelopes of the voltage and current spectra of a CHB with SHE/SHC. They are derived from (21) and (22). The corner frequency is $K\omega_g/N$ as shown by the harmonic order in (21). When $K = N$, each HB switches only once within one period. The modulation is known as staircase modulation and the converter would reach the minimal switching loss.

D. Harmonic Comparison and the Features of an HB With SPWM, SHE/SHC and a CHB With SHE/SHC

This section will compare the harmonics from different topologies and different modulation techniques. Three features of the harmonics are discussed: the controllable frequency range, the maximum magnitude of controllable harmonics (including the fundamental harmonics) and the maximum magnitude of the uncontrollable harmonics.

The voltage/current envelopes comparison is shown in Fig. 7 with $K = 15$ and $NE = V_{\text{DC}}$. The solid curves represent the

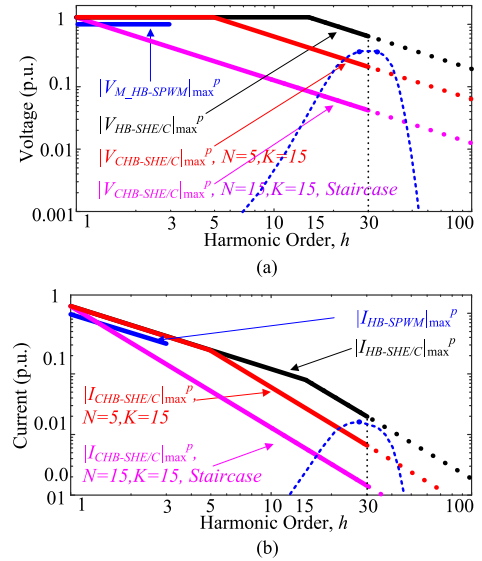


Fig. 7. Comparison of the per unit harmonic envelopes when $K = 15$ and $NE = V_{\text{DC}}$. (a) Voltage. (b) Current.

controllable envelopes, and the dot lines represent the harmonics to be attenuated. Blue, black, red, and pink curves represent different modulation techniques, as shown in Fig. 7.

If the three techniques in Sections III-A–III-C have the same number of switching transitions K , the controllable frequency range of different techniques can be calculated from (13), (18), and (23). The comparison is shown as

$$\begin{aligned} \omega_{\text{CHB-SHE/C-CPS}} &= \omega_{\text{CHB-SHE/C-CPS}} \\ &= 10\omega_{\text{HB-SPWM-CPS}} = 2K\omega_g. \end{aligned} \quad (24)$$

Equation (24) indicates that the SHE/SHC can extend the controllable frequency range to ten times of the SPWM.

For the magnitude of fundamental component, from (8), (16) and (21), an HB or a CHB with SHE/SHC can achieve 127.39% fundamental voltage of an HB with the SPWM technique.

For the voltage magnitude of controllable harmonics, the CHB with SHE/SHC starts to decrease at -20 dB/dec after corner frequency $K\omega_g/N$ as shown in (21). In Fig. 7(a), the blue, pink, and red solid curves show that depending on K/N , a CHB with SHE/SHC can either increase controllable envelope (the red one) or decrease controllable envelope (the pink one) by changing the corner frequency $K\omega_g/N$. This indicates that the voltage magnitudes of the controllable harmonics in a CHB with SHE/SHC can be controlled by changing the number of cascaded cells and the number of switching transitions.

For the current magnitudes of the uncontrollable harmonics, Fig. 7(b) shows that a CHB with SHE/SHC has much lower current harmonics than that of an HB with SPWM at the first significant frequency. The first significant frequency here is defined as the frequency at which the filter is designed based on its harmonic attenuation requirement. In Fig. 7(b), for the HB with SPWM, the first significant frequency is at 29th harmonic frequency and for the CHB with SHE/SHC, it is the first significant frequency is at 31st harmonic frequency. The pink ($N = 15$) and

TABLE II
VOLTAGE/CURRENT COMPARISON

	Controll-able f range	Maximum harmonic magnitude		
		Fundamental component	Controllable harmonics	Uncontrollable harmonics
An HB with SPWM	Small $K\omega_g/5$	Low 1 p.u.	Medium	Medium
An HB with SHE/SHC	Large $2K\omega_g$	High $4/\pi$ p.u.	High	High
A CHB with SHE/SHC	Large $2K\omega_g$	High $4/\pi$ p.u.	Adjustable	Adjustable
A CHB with Staircase	Large $2K\omega_g$	High $4/\pi$ p.u.	Lowest	Lowest

TABLE III
PARAMETERS OF THE NONLINEAR LOAD

R_L / Ω	$C_L / \mu\text{F}$	L_{L1} / mH	L_{L2} / mH
8	100	0.1	5

red ($N = 5$) curves (CHBs with SHE/SHC) have 19.12 dB or 5.12 dB lower uncontrollable harmonics at the first significant frequency than that of the blue curve (HB with SPWM).

The detailed comparison between three topologies and modulation methods is made in Table II. From Table II, a CHB with SHE/SHC has adjustable controllable voltage magnitude, the highest controllable frequency range and the lowest uncontrollable harmonics of the three. It, therefore, has great potential for four-quadrant converter, inverter, APF, and STATCOM applications.

III. PARAMETER DESIGN FOR A CHB WITH SHE/SHC

This section will discuss the critical parameter design for CHBs with SHE/SHC. The parameters include N , E , K , and L_{FLT} . As shown in Fig. 5, the maximum output voltage is NE , which should be smaller than the maximum allowable voltage V_{max} which the grid can withstand. $4NE/\pi$ is the maximum fundamental voltage and shall be larger than the rated output peak voltage V_{rated} . So, NE is limited by a range as

$$\pi V_{\text{rated}}/4 < NE < V_{\text{max}}. \quad (25)$$

Because N is an integer, and E is determined by battery voltage, NE only has a few options within the range of (25). The procedure of designing NE is similar to the design of V_{DC} in an HB. For a fixed NE , the selection of N and E depends on voltage/power ratings, hardware cost, software complexity, etc. If low uncontrollable harmonics is preferred, small E and large N are always preferred as shown in (19).

The general voltage control principle for a CHB with SHE/SHC is shown below based on divided frequency ranges [11], where ω is harmonic frequency

$$\begin{cases} \omega \leq \omega_{\text{CPS}} & v_{\text{CHB-SHE/C}} \text{ is controlled by desired values} \\ \omega_{\text{CPS}} < \omega \leq \omega_{\text{CTRL}} & \text{The voltage references are set as zero} \\ \omega > \omega_{\text{CTRL}} & \text{The harmonics are uncontrollable} \end{cases}$$

where ω_{CPS} is desired maximum compensation frequency, and ω_{CTRL} is maximum controllable frequency.

Equations (26)–(29) shall be satisfied to meet both the compensation capacity criterion and harmonic limitation:

$$\begin{cases} h = 1, & |I_{\text{CHB-SHE/C}}|_{\text{max}} > I_{\text{FUN}} \quad (26) \\ 1 < h \leq H_{\text{CPS}}, & |I_{\text{CHB-SHE/C}}|_{\text{max}} > I_{\text{HAR}} \quad (27) \\ H_{\text{CPS}} < h \leq 2K, & \text{no requirement} \quad (28) \\ h \geq H_{\text{CPS}}, & |I_{\text{CHB-SHE/C}}|_{\text{max}} < I_{\text{STD}} \quad (29) \end{cases}$$

where I_{FUN} and I_{HAR} are the compensation capacity requirements for fundamental and harmonics, respectively, and I_{STD} is the harmonic limitation; where $H_{\text{CPS}} = \omega_{\text{CPS}}/\omega_g$, is the desired maximum compensation harmonic order.

Substituting the first equation of (20) into (26), the maximum inductance $L_{\text{FUN,MAX}}$ for fundamental can be derived

$$L_{\text{FUN,MAX}} = (4NE/\pi - V_g)/(\omega_g I_{\text{FUN}}) \quad (30)$$

where V_g is peak value of grid voltage. As shown in Fig. 7(b), the compensation capacity decreases from $(K/N)\omega_g$. To achieve the maximum compensation capacity within $[0, H_{\text{CPS}}\omega_g]$ and minimize uncontrollable harmonics, K should be chosen as

$$K = NH_{\text{CPS}}. \quad (31)$$

Substituting (31) into (23), the controllable range is $[0, 2NH_{\text{CPS}}\omega_g]$, which is wider than the required compensation frequency range $[0, H_{\text{CPS}}\omega_g]$, which satisfies the frequency condition of the general voltage control principle above.

As in (20), increasing L_{FLT} decreases uncontrollable harmonic and is good to meet the harmonic limitation, but also decreases the compensation capacity. Therefore, harmonic compensation capacity can be used to determine the upper limits $L_{\text{CPS,MAX}}$ of L_{FLT} ; harmonic limit can be used to determine the lower limits $L_{\text{HAR,MIN}}$ of the L_{FLT} . In conclusion, any $L_{\text{FLT}} \in [L_{\text{HAR,MIN}}, \min(L_{\text{FUN,MAX}}, L_{\text{CPS,MAX}})]$ can guarantee that the output current satisfies (26)–(29). The design procedure is shown in Fig. 8.

When $L_{\text{HAR,MIN}} > \min(L_{\text{FUN,MAX}}, L_{\text{CPS,MAX}})$, L_{FLT} has no solutions. In this situation, changing L_{FLT} can never satisfy the compensation capacity and harmonic limitation simultaneously, and redesigning other parameters is inevitable. From (22), increasing N while keeping NE and K/N constant equivalently increases K . This extends controllable frequency range and keeps the current envelope unchanged. Therefore, $L_{\text{FUN,MAX}}$ and $L_{\text{CPS,MAX}}$ are kept unchanged, and $L_{\text{HAR,MIN}}$ is reduced because the controllable frequency range is extended to higher frequencies. In conclusion, increasing N while keeping NE and K/N constant to satisfy $L_{\text{HAR,MIN}} < \min(L_{\text{FUN,MAX}}, L_{\text{CPS,MAX}})$ is a possible solution. From (22), increasing K only can either increase $L_{\text{HAR,MIN}}$ due to increased uncontrollable harmonics magnitude, or decrease $L_{\text{HAR,MIN}}$ due to the extended controllable frequency range. It does not change the compensation capacity ($L_{\text{CPS,MAX}}$ unchanged). So, the relationship between K and $L_{\text{HAR,MIN}}$ is complicated as shown in Fig. 9. Therefore, only increasing K is not recommended.

The detailed procedure to determine the critical parameters is shown in Fig. 8. Compared with the conventional techniques,

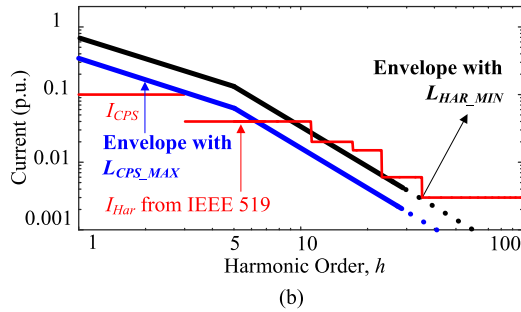
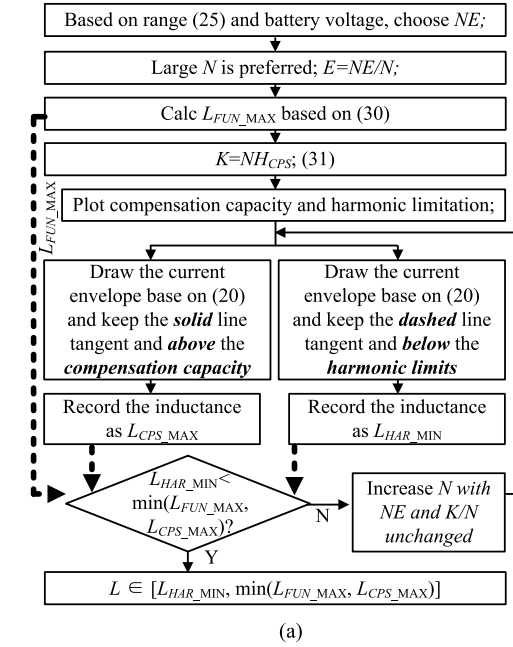


Fig. 8. Flow chart for parameter design. (a) Design flow chart. (b) Illustration of L_{CPS_MAX} and L_{HAR_MIN} .

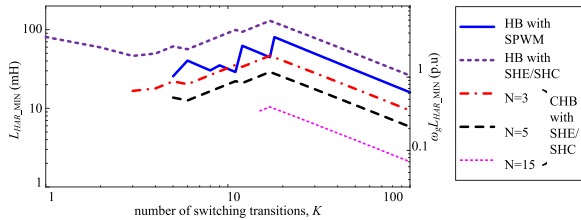


Fig. 9. Minimal inductance versus K to comply with IEEE 519.

the proposed guideline uses polylines to determine how each parameter influences the output current. Moreover, using the current envelope to decide the parameter boundary is quick and straight-forward. The proposed guideline can easily identify the issue if compensation capacity and harmonic limits cannot be met at the same time. Iterations in Fig. 8(a) are only used to find the optimized parameters when this issue happens.

L_{HAR_MIN} s with different topologies and modulation techniques as a function of K calculated from Fig. 8 are compared in Fig. 9 for minimal filter size comparison. The design parameters are: $V_{DC} = NE = 240$ V, $I_L = 20$ A (14.15 A RMS value), the base value is $V_{base} = 240$ V, $I_{base} = 20$ A; $Z_{base} = V_{base}/I_{base} = 12$ Ω . The harmonic

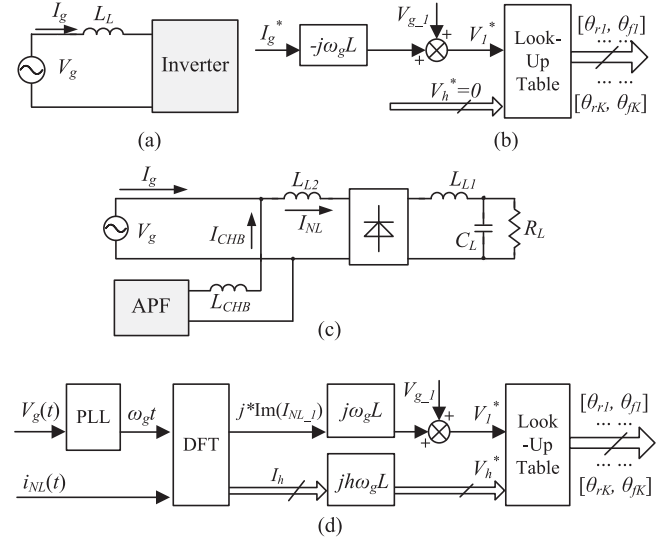


Fig. 10. Topologies and control blocks for simulations and experiments. (a) CHB with SHE when works as an inverter. (b) Control diagram for a CHB with SHE. (c) CHB with SHC when works as an APF. (d) Control diagram for a CHB with SHC.

limits are from IEEE 519. The curve of N Cell CHB starts at $K = N$ because each cell should switch at least once per fundamental period. Similarly, the curve of an HB with SPWM starts at $K = 5$ because the controllable range starts at $K\omega_g/5$, which should be larger than ω_g , as in (13). Fig. 9 shows that increasing N while keeping K unchanged can greatly reduce L_{HAR_MIN} . When K is small, the relationship between K and L_{HAR_MIN} is not monotonous. L_{HAR_MIN} of CHBs with SHE/SHC with large N is much smaller than those of conventional HBs with SPWM and single HBs with SHE/SHC.

IV. SIMULATION AND EXPERIMENT VERIFICATION

Simulations and experiments were conducted on an 110 V/60 Hz, 14 A system to validate the developed design guideline for both CHB SHE and SHC applications. The circuit topology is shown in Fig. 10. Fig. 10(a) and (b) shows a grid-tied CHB working as an inverter with SHE and its control block. Fig. 10(c) shows a CHB working as an APF to compensate the harmonics generated by nonlinear load on the grid and to correct the grid power factor at the same time. Its control block is in Fig. 10(d). Both the control blocks in Fig. 10(b) and (d) are essentially the current mode control with an open-loop control structure. Because the harmonic envelopes in Fig. 6 and the design procedure in Fig. 8 are independent from the control structures, the critical parameter design does not depend on the control structures. It can be applied to voltage mode control, too. Simulations were conducted in MATLAB Simulink. IEEE 519 harmonic limitation was used.

For the grid-tied inverter in Fig. 10(a), the maximum allowable voltage V_{max} , is limited by the both voltage rating of devices and the standard requirements on the grid. For example, NEC article 690.7(C) on solar PV systems requires that for one- and two-family dwellings, the maximum PV system voltage is limited to 600 V [21]. For a four-quadrant inverter,

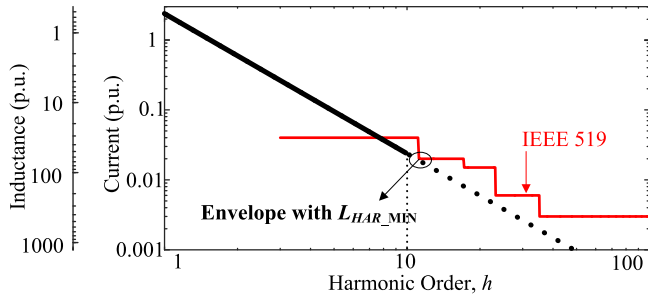


Fig. 11. Envelope of current spectrum to identify L_{HAR_MIN} .

the rated voltage V_{rated} should be larger than the sum of grid voltage V_g and the voltage drop V_L across the inductor. It is assumed that the $N \leq 5$ and $K \leq 30$. As shown in Fig. 9, the minimal impedance of inductor $L_{HAR_MIN}^p$ is 0.48 p.u. Therefore, $V_L = 0.48 NE$, and $V_{rated} \geq (V_g + 0.48 NE)$. From (25), $\pi(V_g + 0.48 NE)/4 < NE < 600$, hence, $202 < NE < 600$. In the experiment, the voltage of single battery is 12 V, so the number of batteries is between 16.8 and 50. In this paper, the smallest possible $NE = 240$ V with 20 batteries was used to reduce the magnitude of uncontrollable harmonics based on (20) and to reduce the system cost. $N = 5$ and $E = 48$ V i.e., four batteries in series for each cell. Based on (30), $L_{FUN_MAX} = 20.04$ mH (0.63 p.u.). Because only fundamental component need to be controllable for the inverter in Fig. 10(a), $H_{CPS} = 1$. From (31), $K = 5$. Based on the dashed current envelope tangent and below the IEEE 519 in Fig. 11, L_{HAR_MIN} can be identified as 16.75 mH (0.53 p.u.). The L_{HAR_MIN} can also be derived from Fig. 9. So, the range of L_{FTL} is [16.75 mH, 20.04 mH]. The per unit range of $\omega_g L_{FTL}$ is [0.53, 0.63] with $V_{base} = 240$ V, $I_{base} = 20$ A. Therefore, a 20 mH inductor can meet the compensation capacity and harmonic requirement at the same time.

The simulated waveforms are shown in Fig. 12. The fundamental peak current is $14\sqrt{2} \approx 20$ A, total harmonic distortion (THD) is 1.16%, all the harmonics are below the limit of IEEE 519 and PF equals to 1.0.

Although a five-cell CHB is applied, the CHB voltage in Fig. 12(a) is 9-level instead of the conventional 11-level. This is because asymmetrical four-quadrant modulation technique [5] was applied and in this modulation technique, the voltage of each cell can be either step-up or step-down within the first quadrant, so the output voltages of two cells can be canceled due to its cascaded operation. However, this asymmetrical modulation technique can greatly extend the modulation index range [5].

In Fig. 12(a), even SHE is applied, low-frequency harmonic I_g still exist. This is due to the distortion of V_g . Actual V_g is not ideally sinusoidal. To make sure that simulations can predict the actual grid currents, the V_g used in the simulations in Fig. 12(a) is from the measured data in the experiments. In Fig. 12(a), the third, fifth, and seventh components of V_g are 5.1 V, 2.4 V, and 1.4 V, respectively. The calculated corresponding harmonic currents are 0.15 A (0.7%), 0.04 A (0.2%), and 0.02 A (0.1%), respectively. They match the simulation results in Fig. 12 well.

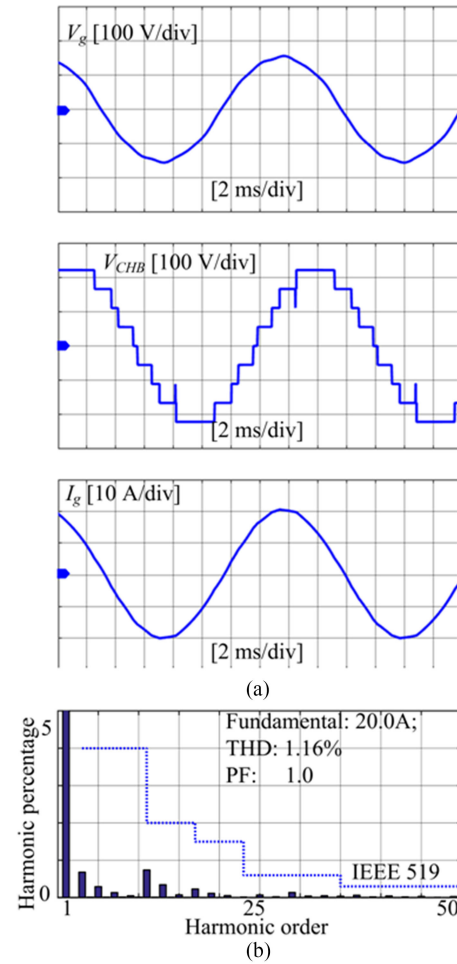


Fig. 12. Simulated results for a CHB with SHE ($M = 0.9$, $N = 5$, $K = 5$). (a) Waveforms. (b) Spectrum of grid current I_g .

Fig. 13 shows the simulated results for a conventional HB using SPWM. The parameters are similar to the CHB with SHE/C case: $V_{DC} = 240$ V, switching frequency is $5f_g$, $M = 0.90$ and $L_{FLT} = 20$ mH. None of the THD and harmonics meet the grid limit. Moreover, Fig. 9 shows that an HB with SPWM requires $L_{HAR_MIN} = 35.7$ mH, which is larger than $L_{FUN_MAX} = 20.04$ mH. As shown in Fig. 13, the current cannot comply with the grid limit and is not applicable for the application.

The comparison between Figs. 12 and 13 validates that with the given parameters ($NE = V_{DC} = 240$ V, $K_{CHB-SHE} = K_{HB-SPWM} = 5$, $L_{CHB} = L_{HB} = 20$ mH), the CHB with SHE has smaller harmonics than those generated by the HB with SPWM. Fig. 9 also illustrates that the HB with SPWM requires to increase the switching frequency to at least $74f_g$ (4440 Hz) with the same inductance 20 mH to comply with the grid limit. Therefore, for applications requiring low-switching frequency and high-power density, multilevel converters with SHE is a promising technique. This conclusion is obvious. Figs. 12 and 13 verified Fig. 9.

As shown in Fig. 13, the major harmonics locate around $10\omega_g$ due to the sideband harmonics of $v_{HB-SPWM}$. From (1), the 7th, 9th, 11th, 13th harmonic of V_{CHB} can be calculated as 42 V, 61 V, 61 V, and 42 V, respectively. Therefore, the

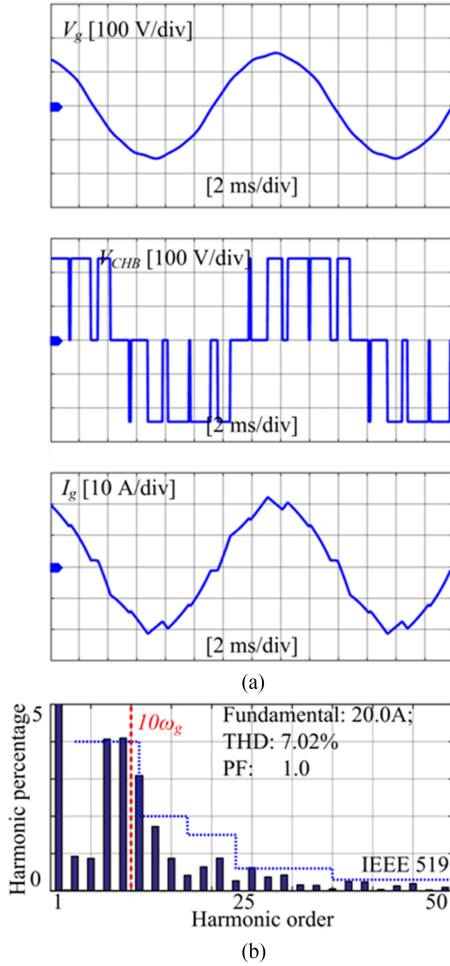


Fig. 13. Simulated results for an HB with SPWM (with $M = 0.9$, $f_{sw} = 5f_g$). (a) Waveforms. (b) Spectrum of grid current I_g .

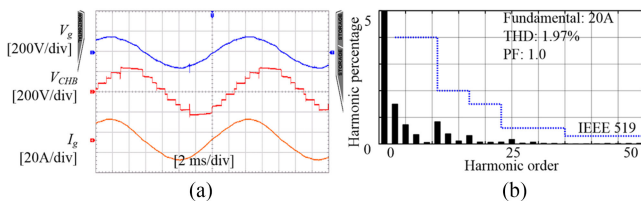


Fig. 14. Experimental results for a CHB with SHE ($M = 0.9$, $N = 5$, $K = 5$). (a) Waveforms. (b) Spectrum of grid current I_g .

corresponding currents are 0.8 A (4%), 0.9 A (4.5%), 0.7 A (3.5%), and 0.4 A (2%). The simulation matches the calculation with only 0.5% difference. Other harmonics above 13th of I_g are relatively small, and they are caused by both the grid voltage distortions and the sideband harmonics of V_{CHB} .

Fig. 14 shows the experimental results corresponding to Fig. 12. The simulated and experimental results match well, and the differences between the simulated and measured of each order of harmonics are within 0.8%. These differences can be caused by the inaccuracy of switching angles, the battery voltages' fluctuation, the nonlinearity of the inductor, and the harmonics of V_g . Zhao and Wang [20] and Moeini *et al.* [23]

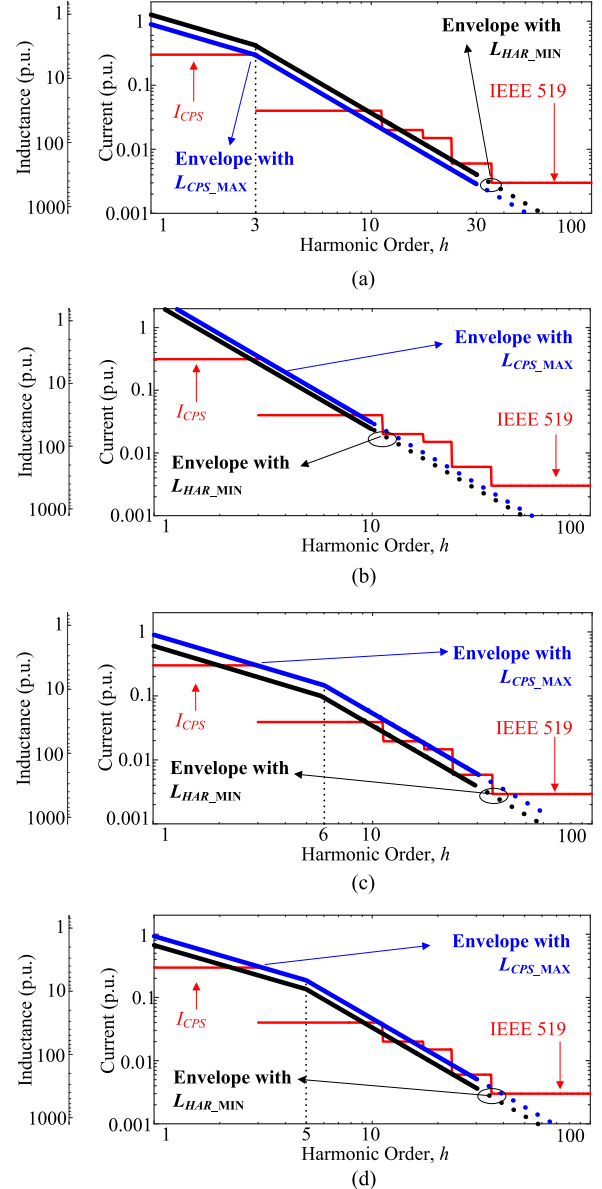


Fig. 15. Current spectrum envelopes with different parameters to identify L_{CPS_MAX} and L_{HAR_MIN} . (a) $N = 5, K = 15$. (b) $N = 5, K = 5$. (c) $N = 5, K = 30$. (d) $N = 3, K = 15$.

derives the analytical solution to explain how the variation of each parameter would affect the output current. Because the current harmonics generated by the nonideality above are low, and they can be compensated actively [11], [12], the effects of nonideality on the parameter design are not discussed in the paper.

Experimental results corresponding to the HB with SPWM are not given because this paper mainly focuses on the critical parameter design for the CHB with SHE/SHC.

Fig. 10(b) is an APF application to compensate the third- and fifth-order harmonics. The compensation capacity is 30% of the rated system current, $I_{FUN} = I_{CPS} = 0.3 I_{rate} = 6$ A (RMS value 4.23 A). The critical parameters were designed based on the flowchart in Fig. 8: $NE = 240$ V based on (25);

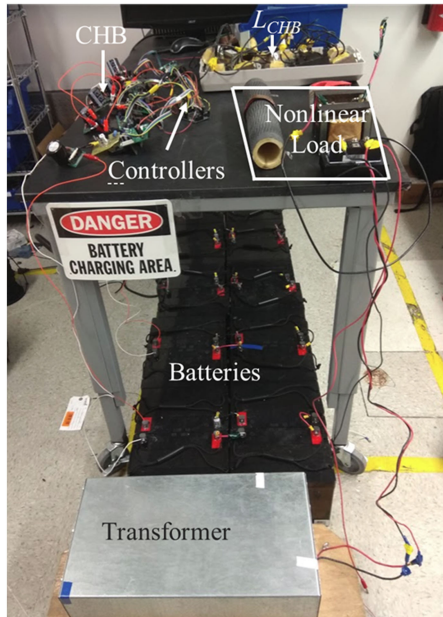


Fig. 16. Hardware prototype of a CHB when works as an APF.

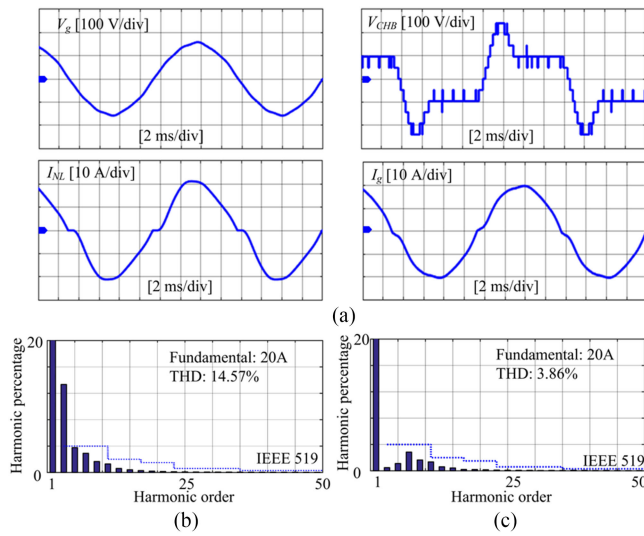


Fig. 17. Simulation results for the single-phase APF ($N = 5, K = 15$). (a) Waveforms. (b) Spectrum of nonlinear load current I_{NL} . (c) Spectrum of grid current I_g .

the maximum N is 5, $E = 48$ V; because $H_{CPS} = 3, K = 15$. $L_{FUN_MAX} = 66.3$ mH (2.08 p.u.) based on (30); $L_{CPS_MAX} = 44.6$ mH (1.39 p.u.) and $L_{HAR_MIN} = 32.6$ mH (1.02 p.u.) can be derived based on Fig. 15(a). The range of the inductor is $L_{FTL} \in [32.6 \text{ mH}, 44.6 \text{ mH}]$, $\omega_g L_{FTL} \in [1.02, 1.39]$ p.u. with $V_{base} = 240$ V, $I_{base} = 20$ A. 35 mH is selected. Fig. 16 shows the hardware prototype corresponding to Fig. 10(c). Fig. 17 shows the simulation results. Fig. 15(b)–(d) illustrate that if parameters are not designed with the proposed guideline, adjusting inductance L_{FLT} may never meet the compensation capacity and harmonic limits simultaneously. In Fig. 15(b), N is unchanged while K is decreased; in Fig. 15(c), N is unchanged while K

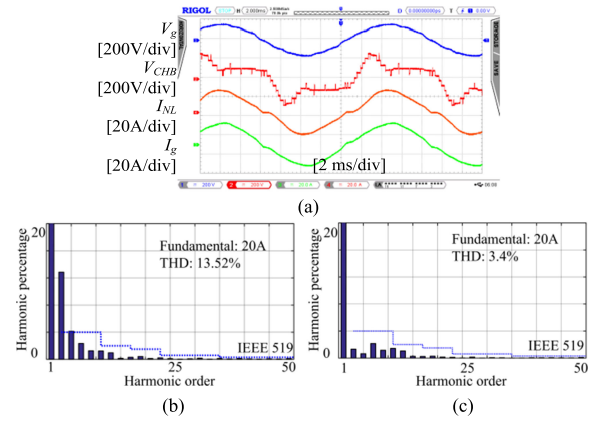


Fig. 18. Experimental results for the single-phase APF ($N = 5, K = 15$). (a) Waveforms. (b) Spectrum of nonlinear load current I_{NL} . (c) Spectrum of grid current I_g .

is doubled; in Fig. 15(d), K is the unchanged while N is decreased. In these cases, L_{CPS_MAX} is smaller than L_{HAR_MIN} , so adjusting L_{FLT} can never meet the compensation capacity and harmonic limits simultaneously. The effect of increasing N is not discussed in this paper because it is assumed that N has a limit.

With the APF design, the power factor is improved from 0.94 (lagging) to 0.99 (lagging); the third harmonic is reduced from 13.2% to 0.5%; and the THD is reduced from 14.57% to 3.86%. Furthermore, after compensation, both the controllable harmonics and the uncontrollable harmonics are below the grid limit, which proves that the proposed design technique can meet both the compensation and attenuation requirements. In Fig. 17, the third and fifth harmonics still exist because of the distortion on V_g . Uncontrollable harmonics still exist.

The proposed technique is further validated in experiments. A five-cell four-quadrant CHB converter is developed in Fig. 16. A TMS320F28335 DSP with a CPLD EP2C5T144C8 are used as the controller in the prototype. The experimental waveforms were recorded with an Rigol MSO 4504 digital oscilloscope. Fig. 18 matches Fig. 17, which further validates that the APF designed with the proposed technique is effective and can meet both the compensation and attenuation requirements.

V. CONCLUSION

A critical parameter design technique for a CHB with SHE/SHC was developed in this paper. The contributions of this paper are as follows.

- 1) The influence of the critical parameters, topologies and modulation techniques to the harmonic envelope was analyzed. The controllable frequency range and the magnitudes of the fundamental, controllable harmonics, and uncontrollable harmonics are explored.
- 2) The minimal filter inductances for an H-Bridge with SPWM, an H-Bridge (HB) with SHE/SHC and a CHB with SHE/SHC have been compared.
- 3) Both the compensation and attenuation requirements are incorporated in the proposed design.

- 4) The design procedure is based on the harmonic envelope, which is simple and intuitive and can be used to evaluate the minimal filter.
- 5) The design technique can be applied to both inverters/converters and APFs, and has been verified by both simulations and experiments.

APPENDIX MAXIMUM VOLTAGE OF A HB AND A CHB CIRCUIT WITH SHE/SHC

A. HB With SHE/SHC

The topology and waveform are shown in Fig. 3, and the equation of the time domain waveform is given by

$$v_{\text{HB-SHE/C}}(t) = \begin{cases} V_{\text{DC}}, & \theta_1 < \omega t < \theta_2, \dots, \theta_{2K-1} < \omega t < \theta_{2K}, \dots \\ 0, & 0 < \omega t < \theta_1, \dots, \theta_2 < \omega t < \pi + \theta_{2K-1}, \dots \\ -V_{\text{DC}}, & \pi + \theta_1 < \omega t < \pi + \theta_2, \dots \end{cases} \quad (\text{A1})$$

The voltage spectrum envelope can be derived with Fourier series as shown

$$v_{\text{HB-SHE/C}}(t) = \sum_{h=1}^{\infty} \left(a_{\text{HB-SHE/C-h}} \cos(h\omega_g t) + b_{\text{HB-SHE/C-h}} \sin(h\omega_g t) \right) = \sum_{h=1}^{\infty} c_{\text{HB-SHE/C-h}} \cos(h\omega_g t + \theta_h) \quad (\text{A2})$$

$$\begin{cases} a_{\text{HB-SHE/C-h}} = 2/T_g \times \int_0^{T_g} v_{\text{HB-SHE/C}}(t) \cos(h\omega_g t) dt \\ b_{\text{HB-SHE/C-h}} = 2/T_g \times \int_0^{T_g} v_{\text{HB-SHE/C}}(t) \sin(h\omega_g t) dt \end{cases} \quad (\text{A3})$$

where $a_{\text{HB-SHE-h}}$ and $b_{\text{HB-SHE-h}}$ are the magnitudes of cosine and sine components of the h th order voltage harmonic, respectively; $c_{\text{HB-SHE/C-h}}$ and θ_h are the magnitude and phase of the h th order voltage harmonic, respectively.

The value of $c_{\text{HB-SHE/C-h}}$ can be calculated by

$$c_{\text{HB-SHE/C-h}} = 2/T_g \times \int_0^{T_g} v_{\text{HB-SHE/C}}(t) \cos(h\omega_g t + \theta_h) dt \quad (\text{A4})$$

The envelope of the maximum voltage is given by

$$\begin{aligned} |c_{\text{HB-SHE/C-h}}| &\leq 2/T_g \\ &\times \int_0^{T_g} |v_{\text{HB-SHE/C}}(t)| |\cos(h\omega_g t + \theta_h)| dt \\ &\leq \frac{2}{T_g} V_{\text{DC}} \int_0^{T_g} |\cos(h\omega_g t + \theta_h)| dt = \frac{4V_{\text{DC}}}{\pi}. \end{aligned} \quad (\text{A5})$$

On the other hand, substituting (A1) to (A3), $a_{\text{HB-SHE/C-h}}$ and $b_{\text{HB-SHE/C-h}}$ of Fourier series can be calculated as

$$\begin{cases} a_{\text{HB-SHE/C-h}} = -\frac{2V_{\text{DC}}}{\pi h} \left(\sum_{i=1}^K (\sin(h\theta_{ir}) - \sin(h\theta_{if})) \right) \\ b_{\text{HB-SHE/C-h}} = \frac{2V_{\text{DC}}}{\pi h} \left(\sum_{i=1}^K (\cos(h\theta_{ir}) - \cos(h\theta_{if})) \right) \end{cases} \quad (\text{A6})$$

where θ_{ir} is the angle of the i th rising edge and θ_{if} is the angle of the i th falling edge.

If $V_{\text{HB-SHE/C-h}}$ is defined as a complex voltage as

$$\begin{aligned} V_{\text{HB-SHE/C-h}} &= b_{\text{HB-SHE/C-h}} + ja_{\text{HB-SHE/C-h}} \\ &= \frac{2V_{\text{DC}}}{\pi h} \left(\sum_{i=1}^K (\cos(h\theta_{ir}) - j \sin(h\theta_{ir})) - \sum_{i=1}^K (\cos(h\theta_{if}) - j \sin(h\theta_{if})) \right) \\ &= \frac{2V_{\text{DC}}}{\pi h} \sum_{i=1}^K (e^{-jh\theta_{ir}} - e^{-jh\theta_{if}}) \end{aligned} \quad (\text{A7})$$

The envelope of the maximum magnitude of $|V_{\text{HB-SHE/C-h}}|$ is given by

$$\begin{aligned} |V_{\text{HB-SHE/C-h}}| &\leq \frac{2V_{\text{DC}}}{\pi h} \sum_{i=1}^K (|e^{-jh\theta_{ir}}| + |e^{-jh\theta_{if}}|) \\ &\leq \frac{4V_{\text{DC}}K}{\pi h}. \end{aligned} \quad (\text{A8})$$

The equality holds and only holds when $h\theta_{1r} = h\theta_{2r} + 2k\pi = \dots = h\theta_{Kr} + 2k\pi = h\theta_{1f} + k\pi = h\theta_{2f} + k\pi = \dots = h\theta_{Kf} + k\pi$.

The harmonic order boundary between constraints (A5) and (A8) can be derived by equating (A5) and (A8). It is found as $h = K$. The maximum voltage is, therefore, given by,

$$|V_{\text{HB-SHE/C}}|_{\text{max}} = \begin{cases} 4V_{\text{DC}}/\pi, & h \leq K \\ 4KV_{\text{DC}}/h\pi, & h \geq K \end{cases}. \quad (\text{A9})$$

B. CHB With SHE/SHC

As shown in Fig. 5, the dc-bus voltage is E and the number of the cells is N , the CHB's maximum dc-output voltage is NE .

Similar to (A4), the magnitude of $c_{\text{CHB-SHE/C-h}}$ is

$$\begin{aligned} c_{\text{CHB-SHE/C-h}} &= 2/T_g \\ &\times \int_0^{T_g} v_{\text{CHB-SHE/C}}(t) \cos(h\omega_g t + \theta_h) dt \end{aligned} \quad (\text{A10})$$

The maximum value is limited by dc voltage limits

$$|c_{\text{CHB-SHE/C-h}}| \leq 4NE/\pi. \quad (\text{A11})$$

If the total number of switching transitions in half fundamental period is K , similar to (A7), the complex voltage is

$$V_{\text{CHB-SHE/C-h}} = \frac{2E}{\pi h} \sum_{i=1}^K (e^{-jh\theta_{ir}} - e^{-jh\theta_{if}}). \quad (\text{A12})$$

Similar to (A8), the envelope of the output voltage of CHB is

$$|V_{\text{CHB-SHE/C}}| \leq 4KE/(h\pi). \quad (\text{A13})$$

The voltage is limited by both (A12) and (A13), the maximum voltage is, therefore, given by

$$|V_{\text{CHB-SHE/C}}|_{\text{max}} = \min\left(\frac{4KE}{h\pi}, \frac{4NE}{\pi}\right) = \begin{cases} 4NE/\pi, & h < K/N \\ 4KE/(h\pi), & h \geq K/N \end{cases}. \quad (\text{A14})$$

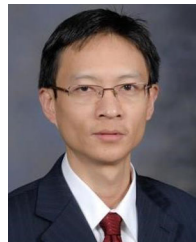
REFERENCES

- [1] M. S. A. Dahidah, G. Konstantinou, and V. G. Agelidis, "A review of multilevel selective harmonic elimination PWM: Formulations, solving algorithms, implementation and applications," *IEEE Trans. Power Electron.*, vol. 30, no. 8, pp. 4091–4106, Aug. 2015.
- [2] J. I. Leon, S. Vazquez, and L. G. Franquelo, "Multilevel converters: Control and modulation techniques for their operation and industrial applications," *Proc. IEEE*, vol. 105, no. 11, pp. 2066–2081, Nov. 2017.
- [3] Y. Yu, G. Konstantinou, C. D. Townsend, R. P. Aguilera, and V. G. Agelidis, "Delta-connected cascaded H-bridge multilevel converters for large-scale photovoltaic grid integration," *IEEE Trans. Ind. Electron.*, vol. 64, no. 11, pp. 8877–8886, Nov. 2017.
- [4] H. Zhao, T. Jin, S. Wang, and L. Sun, "A real-time selective harmonic elimination based on a transient-free inner closed-loop control for cascaded multilevel inverters," *IEEE Trans. Power Electron.*, vol. 31, no. 2, pp. 1000–1014, Feb. 2016.
- [5] H. Zhao and S. Wang, "A four-quadrant modulation technique to extend modulation index range for multilevel selective harmonic elimination/compensation using staircase waveforms," *IEEE J. Emerging Sel. Top. Power Electron.*, vol. 5, no. 1, pp. 233–243, Mar. 2016.
- [6] W. Jin and D. Ahmadi, "A precise and practical harmonic elimination method for multilevel inverters," *IEEE Trans. Ind. Appl.*, vol. 46, no. 2, pp. 857–865, Mar./Apr. 2010.
- [7] L. G. Franquelo, J. Napoles, R. C. P. Guisado, J. I. Leon, and M. A. Aguirre, "A flexible selective harmonic mitigation technique to meet grid codes in three-level PWM converters," *IEEE Trans. Ind. Electron.*, vol. 54, no. 6, pp. 3022–3029, Dec. 2007.
- [8] J. Napoles *et al.*, "Selective harmonic mitigation technique for cascaded H-bridge converters with nonequal DC link voltages," *IEEE Trans. Ind. Electron.*, vol. 60, no. 5, pp. 1963–1971, May 2013.
- [9] A. Moeini, H. Zhao, and S. Wang, "Improve control to output dynamic response and extend modulation index range with hybrid selective harmonic current mitigation-PWM and phase-shift-PWM for four-quadrant cascaded H-bridge converters," *IEEE Trans. Ind. Electron.*, vol. 64, no. 9, pp. 6854–6863, Sep. 2017.
- [10] Y. Chu, S. Wang, and R. Crosier, "Grid active power filters using cascaded multilevel inverters with direct asymmetric switching angle control for grid support functions," in *Proc. Appl. Power Electron. Conf. Expo.*, 2013, pp. 1332–1338.
- [11] H. Zhou, Y. W. Li, N. R. Zargari, Z. Cheng, R. Ni, and Y. Zhang, "Selective harmonic compensation (SHC) PWM for grid-interfacing high-power converters," *IEEE Trans. Power Electron.*, vol. 29, no. 3, pp. 1118–1127, Mar. 2014.
- [12] H. Zhao and S. Wang, "A real-time selective harmonic compensation (SHC) based on asymmetric switching angle modulation and current feedback control for cascaded modular multilevel inverters," in *Proc. IEEE Appl. Power Electron. Conf. Expo.*, Mar. 15–19, 2015, pp. 2160–2166.
- [13] D. Ahmadi and W. Jin, "Online selective harmonic compensation and power generation with distributed energy resources," *IEEE Trans. Power Electron.*, vol. 29, no. 7, pp. 3738–3747, Jul. 2014.
- [14] Q. Liu, L. Peng, Y. Kang, S. Tang, D. Wu, and Y. Qi, "A novel design and optimization method of an LCL filter for a shunt active power filter," *IEEE Trans. Ind. Electron.*, vol. 61, no. 8, pp. 4000–4010, Aug. 2014.
- [15] Y. Jiao and F. C. Lee, "LCL filter design and inductor current ripple analysis for a three-level NPC grid interface converter," *IEEE Trans. Power Electron.*, vol. 30, no. 9, pp. 4659–4668, Sep. 2015.
- [16] A. A. Rockhill, M. Liserre, R. Teodorescu, and P. Rodriguez, "Grid-filter design for a multimewatt medium-voltage voltage-source inverter," *IEEE Trans. Ind. Electron.*, vol. 58, no. 4, pp. 1205–1217, Apr. 2011.
- [17] M. Zabaleta, E. Burguete, D. Madariaga, I. Zubimendi, M. Zubiaga, and I. Larrazabal, "LCL grid filter design of a multimewatt medium-voltage converter for offshore wind turbine using SHEPWM modulation," *IEEE Trans. Power Electron.*, vol. 31, no. 3, pp. 1993–2001, Mar. 2016.
- [18] M. Liserre, F. Blaabjerg, and S. Hansen, "Design and control of an LCL-filter-based three-phase active rectifier," *IEEE Trans. Ind. Appl.*, vol. 41, no. 5, pp. 1281–1291, Sep./Oct. 2005.
- [19] D. G. Holmes and T. A. Lipo, *Pulse Width Modulation for Power Converters: Principles and Practice*. New York, NY, USA: Wiley, 2003.
- [20] H. Zhao and S. Wang, "Investigation of CCL filter for multilevel selective harmonic compensation (SHC)," in *Proc. IEEE Energy Convers. Congr. Exposition*, 2017, pp. 5206–5213.
- [21] Solar Photovoltaic (PV) System, National Electric Code Article 690, 2017.
- [22] P. Channegowda and V. John, "Filter optimization for grid interactive voltage source inverters," *IEEE Trans. Ind. Electron.*, vol. 57, no. 12, pp. 4106–4114, Dec. 2010.
- [23] A. Moeini, H. Zhao, and S. Wang, "A current reference based selective harmonic current mitigation PWM technique to improve the performance of cascaded H-bridge multilevel active rectifiers," *IEEE Trans. Ind. Electron.*, vol. 6, no. 1, pp. 727–737, Jan. 2016.



Hui Zhao (S'14) received the bachelor's and master's degrees in electrical engineering from the Huazhong University of Science and Technology, Wuhan, China, in 2010 and 2013, respectively, and the Ph.D. degree in power electronics from the University of Florida, Gainesville, FL, USA in 2018.

He had an internship at General Electric (GE) Global Research Center (GRC) in 2013. He has authored or coauthored more than 20 IEEE journal and conference papers. His research interests include the modeling and optimization of magnetic components, electrical vehicle charging, and multilevel converters.



Shuo Wang (S'03–M'06–SM'07) received the Ph.D. degree in electrical engineering from Virginia Tech, Blacksburg, VA, USA, in 2005.

Since 2015, he has been an Associate Professor with the Department of Electrical and Computer Engineering, University of Florida, Gainesville, FL, USA. From 2010 to 2014, he was with the University of Texas at San Antonio, TX, USA, first as an Assistant Professor and later as an Associate Professor. From 2009 to 2010, he was a Senior Design Engineer in GE Aviation Systems, Vandalia, OH, USA. From 2005 to 2009, he was a Research Assistant Professor with Virginia Tech. He has authored or coauthored more than 160 IEEE journal and conference papers and holds eight US patents.

Dr. Wang was the recipient of Best Transaction Paper Award from the IEEE Power Electronics Society in 2006 and two William M. Portnoy Awards for the papers published in the IEEE Industry Applications Society in 2004 and 2012, respectively, and the prestigious National Science Foundation CAREER Award in 2012. He is currently an Associate Editor for the IEEE TRANSACTIONS ON INDUSTRY APPLICATIONS and a Technical Program Cochair for IEEE 2014 International Electric Vehicle Conference.



Amirhossein Moeini (S'16) received the B.Sc. degree in electrical engineering from the University of Guilan, Rasht, Iran, in 2011, and the M.Sc. degree in power electronics and electrical machines from the University of Tehran, Tehran, Iran, in 2013. He is currently working toward the Ph.D. degree in power electronics at the Power Electronics and Electrical Power Research Laboratory, University of Florida, Gainesville, FL, USA.

His current research interests include modeling and control of power electronic converters, FACTS devices, power quality, evolutionary optimization methods, and optimal modulation techniques.